Very Extended Shapes In ^{108}Cd: Evidence For The Occupation of "Hyper-Intruder" Orbitals

A. Görgen*, R.M. Clark*, P. Fallon*, M. Cromaz*, M.A. Deleplanque*, R.M. Diamond*, G.J. Lane*, I.Y. Lee*, A.O. Macchiavelli*, R.G. Ramos*, F.S. Stephens*, C.E. Svensson*, K. Vetter*, D. Ward*, M.P. Carpenter†, R.V.F. Janssens† and R. Wadsworth**

*Nuclear Science Division, Lawrence Berkeley National Laboratory, Berkeley, California, 94720
†Physics Division, Argonne National Laboratory, Argonne, Illinois, 60439
**Department of Physics, University of York, Heslington, York YO1 5DD, United Kingdom

Abstract. High-spin states in ^{108}Cd were studied following the reaction ^{64}Ni(^{48}Ca,4n) at a beam energy of 207 MeV. Gamma rays were detected using the Gammasphere array. Two rotational bands have been observed at very high angular momentum. Measurements of fractional Doppler shifts yielded lower limits for the quadrupole moments and showed that the observed structures are at least as deformed as the superdeformed structures *e.g.* in the $A \approx 150$ region, and possibly exceed a 2:1 axis ratio. The existence of very extended shapes has been predicted by cranked Strutinsky calculations, and recent projected shell model calculations suggest that the $\pi i_{13/2}$ *hyper-intruder* orbital is occupied in these newly observed bands.

INTRODUCTION

Nuclei with extreme deformation are found in various regions of the nuclear chart. For certain proton and neutron numbers, for example in the fission isomers in the actinide region and in the $A \approx 150$ region around ^{152}Dy, the quadrupole deformation can approach $\varepsilon_2 \approx 0.6$, which corresponds to a major-to-minor axis ratio of $c/a \approx 2$.

In the simple picture of an axially deformed harmonic oscillator one finds shell gaps for all rational axis ratios. Nuclear shapes stabilized by the shell gaps at a 2:1 axis ratio are called superdeformed, while the long-sought-for shapes with an axis ratio of 3:1 are called hyperdeformed.

More realistic models, which include the spin-orbit interaction for example, alter the superdeformed magic numbers (as well as the spherical ones) and also the deformation corresponding to the superdeformed shell gap. In general, the deformations are skewed to lower values, and in the $A \approx 190$ and the $A \approx 130$ region the SD shell gap occurs at $\varepsilon_2 \approx 0.5$ and $\varepsilon_2 \approx 0.45$, respectively.

The spin orbit interaction causes certain high-j orbitals to be lowered in energy so that they are shifted down from one oscillator shell (N) to the next shell (N-1). These intruder states carry large angular momentum and have the largest quadrupole moments. Because intruder states are steeply down-sloping in energy as a function of deformation, they will become occupied at successively lower particle number for increasing deformation. For example, the $\pi i_{13/2}$ orbital is at the Fermi surface among orbitals from the N-1 shell for spherical nuclei at $Z \approx 100$ and for normal-deformed nuclei ($\varepsilon_2 \approx 0.2$) at $Z \approx 90$. As the deformation increases, the $\pi i_{13/2}$ orbital is shifted lower and lower in energy until it intrudes the N-2 shell for superdeformed nuclei around $Z \approx 66$ (*i.e.* the Dy region). In general, the occurrence of superdeformed nuclei can be correlated with the occupation of intruder states originating from not one but two major oscillator shells above. The shift to the next lower shell (N-3) occurs at even greater deformations, close to the 3:1 axis ratio expected for hyperdeformed nuclei. We may therefore expect hyperdeformed nuclei to involve intruder orbitals from three shells above.

It is therefore possible, for a given nucleon number, to classify an intruder state according to the number of shells it has been lowered and the corresponding deformation at which it becomes occupied. The $\pi i_{13/2}$ orbital is a *normal intruder* (N-1) in the Actinide region, a *super-intruder* (N-2) in the rare earth region, and a *hyper-intruder* (N-3) for nuclei around $Z \approx 48$. The $\nu j_{15/2}$ orbital is the corresponding neutron *normal intruder* (N-1), *super-intruder* (N-2),

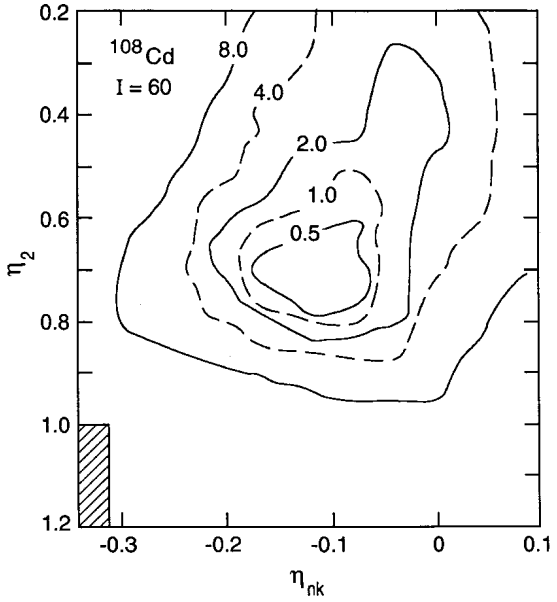

FIGURE 1. Contour plot of the energy surface of ^{108}Cd as a function of the quadrupole deformation parameter η_2 and the necking parameter η_{nk} at $I = 60\,\overline{h}$ [1]. For $\eta_{nk} = 0$ the parameter η_2 becomes the more familiar parameter β_2. The minimum corresponds to an axis ratio of $c/a = 2.3$.

and *hyper-intruder* (N-3) for these three mass regions.

However, to follow an intruder orbital through three major shells to extreme deformations is a large extrapolation, so that predictions of the exact positions of these orbitals and predictions where very extended shapes can be found are unreliable. Both the shell structure and the liquid-drop properties of the nucleus determine whether extreme deformations can occur or not. Recent cranked Strutinsky calculations by Chasman [1] predict many very extended shape minima at high angular momentum in the mass $A \approx 100$ region. These calculations used a four-dimensional shape parameterization taking into account quadrupole, octupole, and hexadecapole deformations, and a necking degree of freedom. The calculated minima become yrast only at very high angular momenta close to the expected fission limit, and, consequently, the barrier to fission is often very small, making experimental observation difficult. Another experimental restriction is that many of the nuclides showing pronounced minima are neutron rich and cannot be reached in a suitable heavy-ion induced fusion-evaporation reaction with stable beams and targets.

From both the theoretical predictions and the experimental possibilities, ^{108}Cd is a promising candidate for investigating very deformed shapes. In the calculations, a pronounced minimum at a deformation corresponding to an axis ratio of $c/a = 2.3$ results from shell corrections for both protons and neutrons. This deformation is significantly larger than those observed for superdeformed bands in other mass regions. This structure is calculated to become yrast at $I \approx 60\,\overline{h}$, and at this angular momentum the height of the fission barrier was 9.1 MeV, implying that any structures populated are likely to survive against fission. A contour plot of the minimum in the plane of the quadrupole deformation parameter and the necking parameter is shown in Fig. 1.

Another cranked Strutinsky calculation by Werner and Dudek [2] using a different shape parameterization predicts a stable secondary minimum at a large deformation of $\beta_2 \approx 0.7$, which develops at a similar angular momentum of $60\,\overline{h}$. This deformation corresponds to an axis ratio of $c/a \approx 1.9$.

EXPERIMENTAL METHODS AND RESULTS

An experiment to search for structures built on very extended shapes in ^{108}Cd was performed at the ATLAS accelerator at Argonne National Laboratory. High-spin states in ^{108}Cd were populated in the reaction ^{64}Ni(^{48}Ca,4n) at a beam energy of 207 MeV. Gamma rays were detected with the Gammasphere detector array which consisted of 101 Compton-suppressed germanium detectors at the time of the experiment. The target comprised a stack of two ^{64}Ni foils with a thickness of 500μg/cm^2 each. Events were written to tape when at least six germanium detectors gave coincident signals after Compton suppression. A total of 1.3×10^9 events were recorded on magnetic tape.

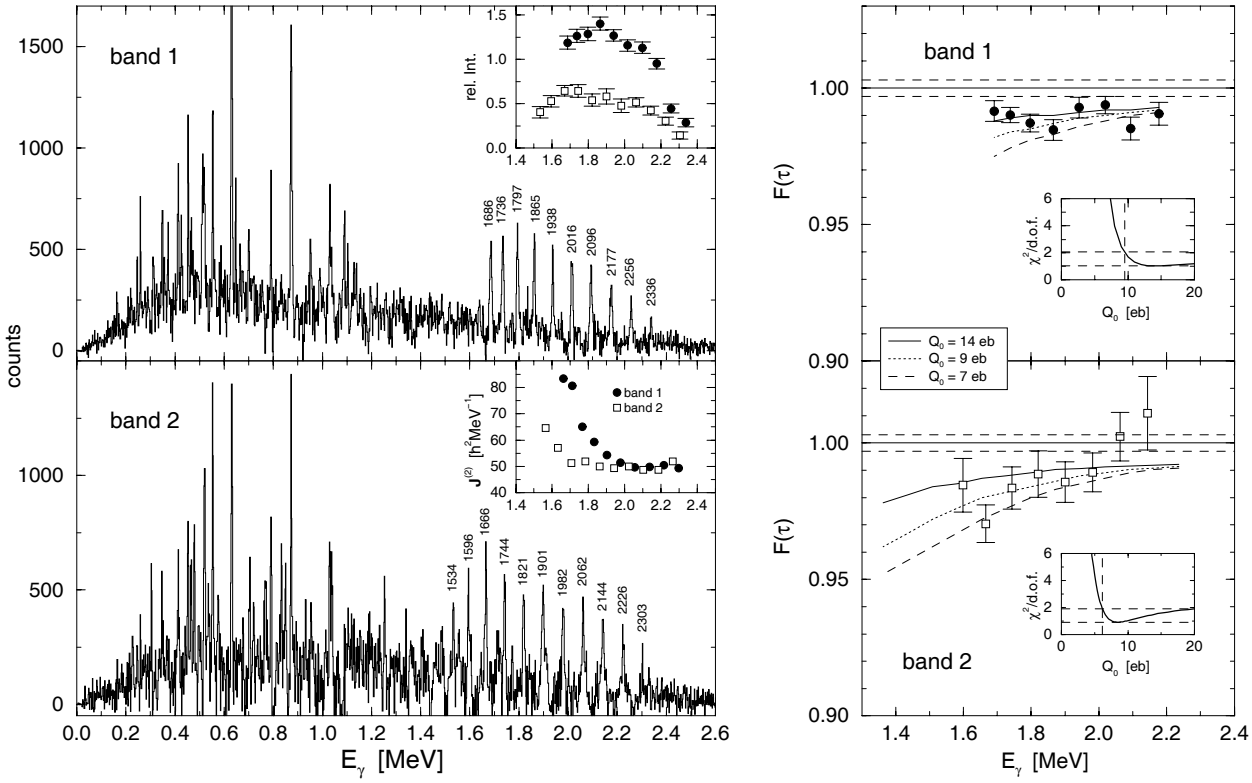

FIGURE 2. The left-hand part of the figure shows spectra of bands 1 and 2, respectively. The spectra were obtained by summing all combinations of double gates on the in-band transitions. In addition, a modular fold of $K \geq 22$ was required. The insets show the relative intensities of the bands with respect to the the total intensity of the reaction channel, and the dynamic moments of inertia, respectively. The values for band 1 are given by the full circles, those for band 2 by the open squares. The right-hand part of the figure shows the results of the fractional Doppler shift analysis. The lines show examples for calculated $F(\tau)$ curves. The χ^2 fits for the calculated curves to the data as a function of the quadrupole moment Q_0 are shown in the insets. The horizontal dashed lines represent the minimal value χ^2_{min} and $\chi^2_{min}+1$. The vertical dashed lines indicate the lower limit of the quadrupole moment consistent with a 1σ error.

In the off-line analysis the data were stored on disk in an indexed, energy-ordered database with the program BLUE [3]. The BLUE database and the accompanying "query" routines provide the capability to create spectra under various gating conditions in multiple dimensions on an interactive or near-interactive time scale. For this analysis the database contained the γ-ray energies, the angles of the detectors in which the γ ray was detected, and the fold of the event. In addition, an E_γ-E_γ-E_γ cube was sorted in order to search for band structures.

Two bands were found by applying a grid search to the cube [4, 5]. The gate conditions were subsequently optimized using the BLUE database, in which events are analyzed in their native fold without breaking up events into sub-events with lower fold. Spectra of bands 1 and 2 are shown in Fig. 2. Both spectra were obtained by summing all combinations of double gates on in-band transitions. To enhance those events that were populated at the highest angular momenta, it was required that a minimum number of Gammasphere modules, K, gave coincident signals. A module of Gammasphere consists of a HPGe detector and its surrounding BGO suppression shield. For the spectra shown in Fig. 2, $K \geq 22$ was required. Although the BGO suppressors were shielded from direct radiation from the target by hevimet collimators, a cut on this modular fold distribution is effective in selecting high-spin events and in reducing the low-spin background, so that the overall quality of the spectra was significantly improved. This is illustrated in Fig. 3 where spectra of band 1 are shown with various cuts on K, both for measurements with collimators on and with the collimators removed.

The assignment of the two bands to ^{108}Cd is based on γ-ray coincidences with low-lying transitions in this nucleus. Bands 1 and 2 carry about 1.4% and 0.6% of the intensity of the $4n$ reaction channel leading to ^{108}Cd, respectively, and this channel was populated with about 15% of the total fusion evaporation cross section. The intensity pattern for

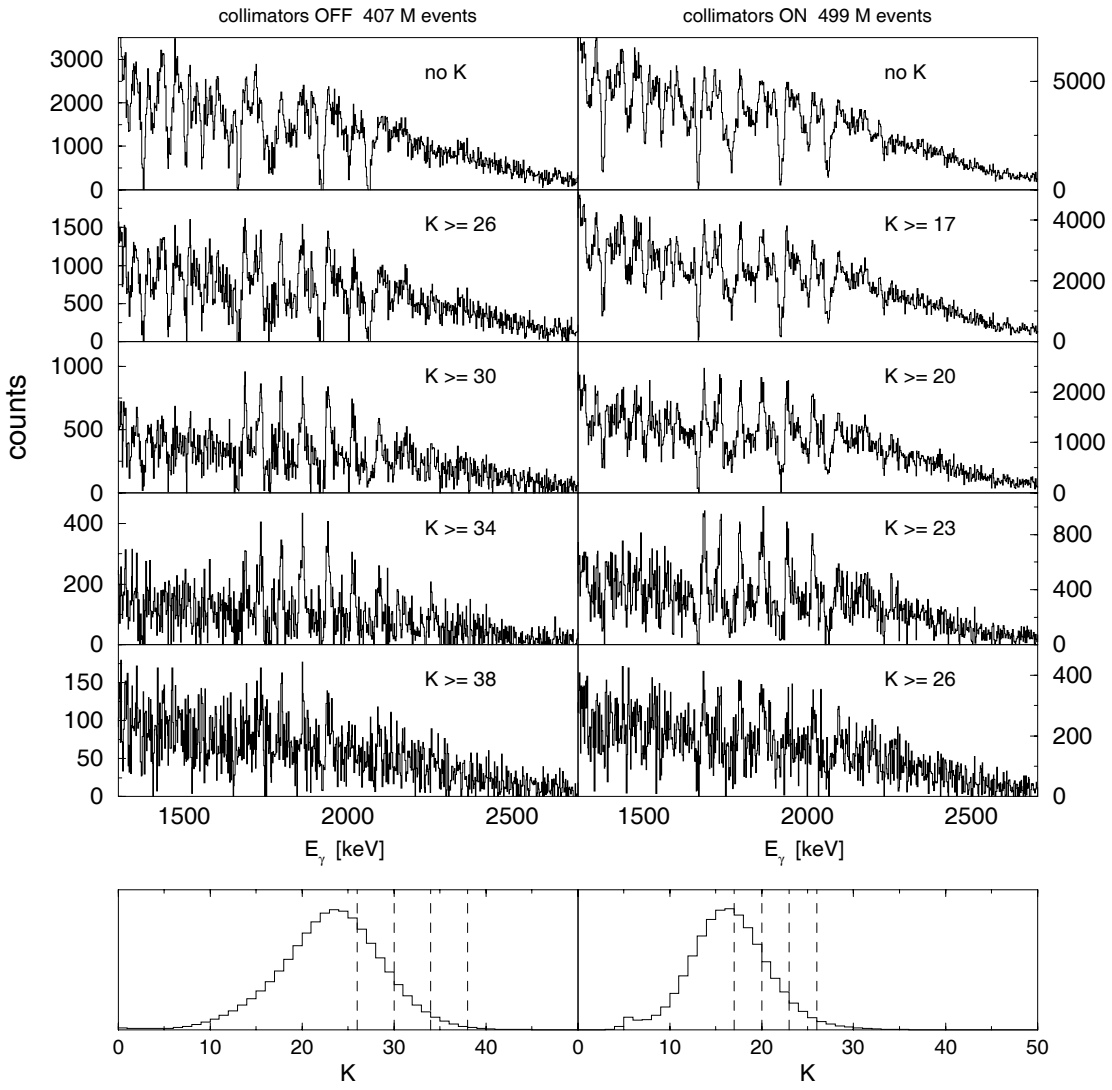

FIGURE 3. The upper part illustrates how the spectrum of the band improves when only events above a certain threshold in the modular fold K are incremented. All spectra were obtained by summing single gates on the in-band transitions. The spectra on the right were recorded during the present experiment in which the BGO suppressors were shielded by hevimet collimators. For comparison, spectra recorded in an earlier experiment [6] in which the collimators were removed in order to get a reliable measurement of the fold and total-energy distributions are shown on the left. In both experiments the same reaction at the same beam energy was used, and the spectra represent roughly the same number of events for both cases. The top panels show the spectra without any condition on K. In the panels below, a more and more restrictive cut on K was performed. These cuts are shown in the bottom spectra of the respective K distributions.

both bands is shown in Fig. 2.

Neither of the bands could be linked to lower-lying states. Therefore the exact spins of the states remain unknown. From the transition energies one can extract the dynamic moment of inertia $\mathcal{J}^{(2)}$. This is also shown in Fig. 2. Both bands show a very similar behavior of the dynamic moment of inertia. At high rotational frequencies $\mathcal{J}^{(2)}$ is constant and of the same magnitude for both bands. At lower frequencies, both bands show a sharp increase in $\mathcal{J}^{(2)}$, which usually indicates a band crossing. Because of this sharp increase it is difficult to estimate the spins from a parameterization of the dynamic moment of inertia in powers of the rotational frequency ω. An estimate for the spins was obtained by assuming that the kinematic moment of inertia $\mathcal{J}^{(1)}$ and the dynamic moment of inertia $\mathcal{J}^{(2)}$ are equal at the highest angular momentum where $\mathcal{J}^{(2)}$ is constant, although there is no *a priori* reason to assume that the nucleus behaves like a rigid rotor. Under these assumptions it is estimated that band 1 lies in the spin range

between 40 $\hbar$ and 60 $\hbar$ and band 2, which is observed to lower frequencies, continues slightly lower in spin. The fact that the bands are strongly enhanced when observed in coincidence with a very large number of γ rays, *e.g.* a number corresponding to the top few percent of the spin distribution, supports the suggestion that the bands lie at very high angular momentum.

In both cases the highest known normal deformed state observed in coincidence with the band is a 16^+ state, leaving a large gap of more than 20 units of angular momentum unobserved. This is rather unusual. For most of the known superdeformed bands the intensity flux is accounted for in the normal deformed level scheme after only a few units of angular momentum, even if discrete linking transitions are not observed.

The in-band transitions are extremely fast and the states decay while the recoiling nucleus traverses the thin target. Residual Doppler shifts were measured for transitions of both bands and the corresponding average recoil velocity for each of the transitions was determined [4, 5]. The fractional Doppler shifts $F(\tau) = \beta/\beta_0$, with β_0 being the average initial recoil velocity, are plotted in the right-hand part of Fig. 2. Since the intensity of band 2 is significantly weaker than the intensity of band 1, the uncertainties are larger for band 2. All $F(\tau)$ values were deduced from analysis of double-gated spectra for the 17 different detector angles of Gammasphere. Besides the statistical error, the uncertainties include the systematic errors associated with different gating conditions and background subtractions. The uncertainty in determining the initial recoil velocity β_0 is indicated by the horizontal dashed lines in the $F(\tau)$ plots. This represents the combined systematic errors assuming a 1 MeV uncertainty in the beam energy and a 10% uncertainty in the target thickness.

Calculated $F(\tau)$ curves are shown for quadrupole moments Q_0 = 7, 9, and 14 eb for both bands. The stopping powers were calculated using the stopping powers of Ziegler *et al.* [7]. The intensities of the side-feeding transitions were fitted to the data, and it was assumed that they have the same quadrupole moment as the in-band transitions. The insets in the right-hand part of Fig. 2 show χ^2 fits of the calculated $F(\tau)$ curves to the data as a function of the quadrupole moment. Since the $F(\tau)$ values for band 1 are essentially flat, the χ^2 curve is very shallow and no reasonable upper limit for the quadrupole moment can be given. A minimum is found at Q_0 = 14 eb with a reduced χ^2_{min} = 1.04. The only reliable number that can be extracted from this measurement is the lower limit for the quadrupole moment of Q_0 = 9.5 eb at $\chi^2_{min} + 1$. The χ^2 fit to the data of band 2 reveals a minimum at Q_0 = 8.5 eb. The lower limit compatible with a 1σ error is Q_0 = 6.2 eb. Again, the χ^2 curve is rather shallow so that no meaningful upper limit can be given for the quadrupole moment. The systematic errors introduced by the choice of the stopping powers are not included and may be as large as 15%.

DISCUSSION

The quadrupole moments measured by the analysis of residual Doppler shifts indicate that the observed bands are built on very deformed structures. The lower limit of the quadrupole moment for band 1, $Q_0 > 9.5e$b, corresponds to an axis ratio of $c/a > 1.8$. This places ^{108}Cd among the most deformed structures ever observed. For example, the corresponding ratios for the yrast bands in ^{152}Dy [8] and ^{236}U [9] are c/a = 1.85 and 1.84, respectively. The possibility that the bands in ^{108}Cd exceed 2:1 deformation cannot be excluded on the basis of the data.

The experimental observations stimulated calculations in the frame of the projected shell model [10] to investigate the structure of the bands [11]. In particular the steep increase of the dynamic moment of inertia towards lower rotational frequencies, indicative of a band crossing, gives a 'handle' on the structure of the bands, and a microscopic description of this behavior can be attempted. The projected shell model is a spherical shell model truncated in a deformed BCS single-particle basis. The basis is constructed from the deformed quasiparticle vacuum and two- and four-quasiparticle states for both protons and neutrons. Relevant orbitals from several major shells (N = 3–7) are included in the basis, and the deformation for the basis states is fixed to $\varepsilon_2 = 0.67$, motivated by the experimental results. The violated rotational symmetry is restored by angular-momentum projection, and the Hamiltonian, including a quadrupole-quadrupole interaction and monopole and quadrupole pairing, is diagonalized in the angular-momentum projected basis. The resulting many-body wave function is a superposition of angular-momentum projected multi-quasiparticle states.

Fig. 4 shows the calculated transition energies and kinematic and dynamic moments of inertia for the yrast sequence, *i.e.* the sequence of states with the lowest energy $E(I)$ for a given angular momentum. The upper part shows the transition energies $E(I) - E(I-2)$ as a function of spin and compares it to the measured transition energies of band 1, for which the spins are not known experimentally. Very good agreement is achieved when the band is placed between I = 36 and 56 $\hbar$. This agrees well with the original estimate of the spin range I = 40 to 60 $\hbar$. The lower part of Fig. 4

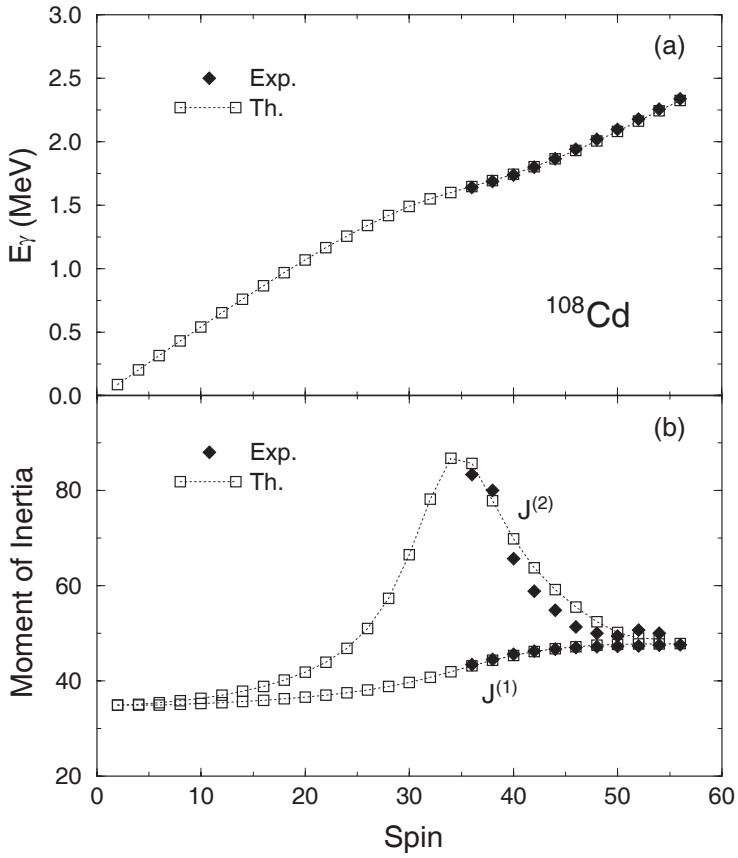

FIGURE 4. The upper panel (a) shows calculated transition energies of the yrast sequence as a function of angular momentum (open symbols). The measured γ-ray energies of band 1 (full symbols) are placed in spin to result in the best agreement with the calculated values. The lower panel (b) shows the calculated kinematic and dynamic moments of inertia for the yrast sequence (open symbols) and the experimental values (full symbols) for band 1 for the assumed spins. The figure is taken from [11].

shows a comparison of calculated and experimental moments of inertia $\mathcal{J}^{(1)}$ and $\mathcal{J}^{(2)}$ under the same assumption for the experimental spins. Again there is very good agreement between theory and experiment, and, most importantly, the steep increase in the dynamic moment of inertia $\mathcal{J}^{(2)}$ towards lower spin is reproduced. This behavior of the moment of inertia can be explained by a band crossing of the $\pi i_{13/2}$ two-quasiparticle band with the zero-quasiparticle band. This is illustrated in Fig. 5.

Fig. 5 shows rotational bands calculated for various configurations for ^{108}Cd (left) and ^{112}Cd (right). The lines represent bands built on pure configurations before different configurations are allowed to mix. The dots represent the states with the lowest energy for a given angular momentum after configuration mixing. The closer a pure configuration lies to the yrast band, the more it dominates the configuration. As can be seen in the left part of Fig. 5, the $\pi i_{13/2}[1/2,3/2]$ two-quasiparticle configuration is clearly lowest at high angular momentum in ^{108}Cd. This configuration crosses the zero-quasiparticle configuration at $I \approx 38\ \hbar$, giving rise to the pronounced increase in the dynamic moment of inertia shown in Fig. 4. Therefore, the $\pi i_{13/2}$ configuration seems to be the dominant configuration of band 1.

This N=6 $\pi i_{13/2}$ orbital is the *normal intruder* (N-1) orbital in the actinide region, it is a *super-intruder* (N-2) around $A \approx 150$, but in ^{108}Cd (where N=3 orbitals are at the Fermi surface at normal deformation) it originates from three shells above and can be classified as a *hyper-intruder*.

In the best cases of superdeformed nuclei, both protons and neutrons occupy *super-intruder* orbitals. In this case, the corresponding neutron *hyper-intruder* in the $A \approx 110$ region would be the $\nu j_{15/2}$ orbital. As can be seen in the left-hand part of Fig. 5, according to the projected shell model calculations for ^{108}Cd, the $\nu j_{15/2}$ orbital lies much higher in energy and does not contribute significantly to the wave function. However, as one moves to more neutron-rich isotopes, this orbital will eventually come down in energy. This is illustrated in the right-hand part of Fig. 5,

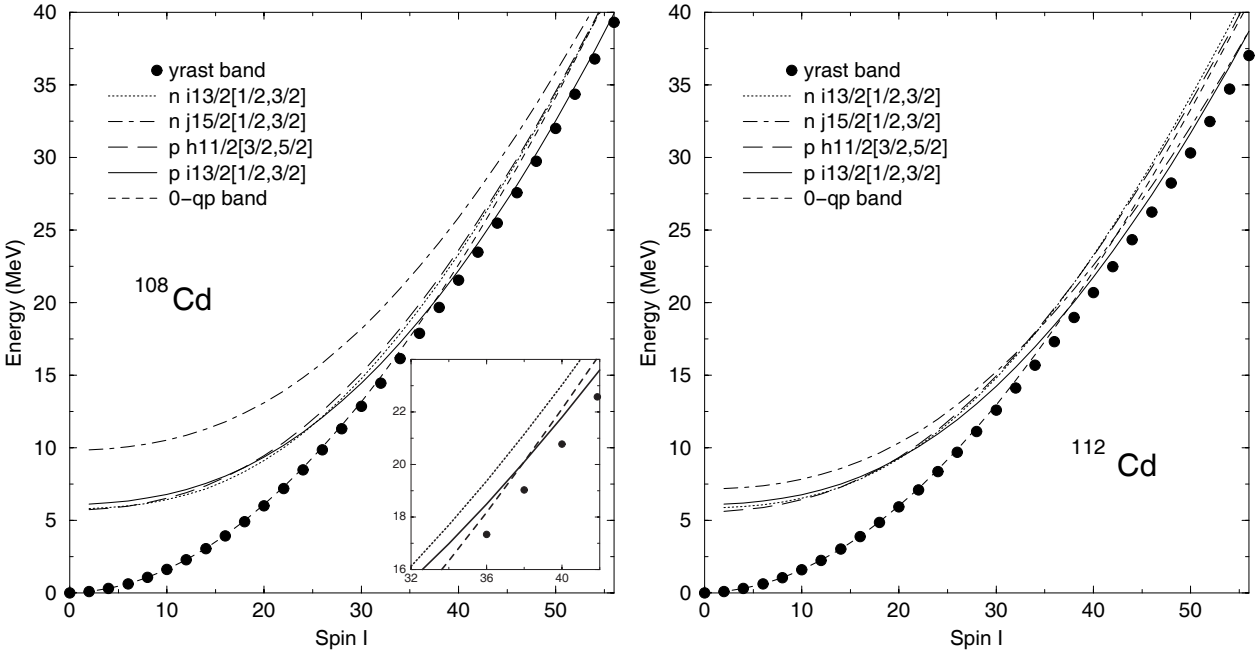

FIGURE 5. Band diagrams for ^{108}Cd (left) and ^{112}Cd (right) [12]. The different-style lines represent the pure bands of some selected basis configurations. The dots show the yrast band, *i.e.* the states lowest in energy for a given spin after configuration mixing. The inset enhances the region where the band crossing is observed experimentally and shows only the lowest configurations for clarity reasons.

were the same plot is shown for ^{112}Cd. There the $\nu j_{15/2}$ orbital lies very close to the $\pi i_{13/2}$, which would make this nucleus an ideal hunting ground for hyperdeformation. Furthermore, with every additional neutron, the nucleus can hold more angular momentum, enhancing the likelihood of populating such structures and reducing the fission competition. Caution is advised since predictions about energies of these orbitals at such extreme deformations are very uncertain. More experimental evidence and additional cases in neighboring nuclei are needed to place calculations on a stronger footing. Unfortunately, ^{108}Cd is the most neutron-rich Cd isotope accessible in a (HI,xn) reaction with stable beams and targets that can bring in enough angular momentum. Heavier isotopes are only accessible with light ions or through an α-evaporation channel, in which case the evaporated α-particle reduces the angular momentum of the residual nucleus.

SUMMARY

We have found two rotational bands in ^{108}Cd at very high angular momentum. Lifetime measurements using the method of fractional Doppler shifts provided a lower limit for the deformation. It is found that the bands are among the most deformed structures ever observed and the possibility of a major-to-minor axis ratio of more than 2:1, which was predicted by cranked Strutinsky calculations for ^{108}Cd, cannot be excluded on the basis of the data. Both bands show a sharp increase of the dynamical moment of inertia toward lower rotational frequencies which is indicative of a band crossing. Microscopic calculations in the frame of the projected shell model are able to reproduce this behavior of the moment of inertia and suggest that band 1 is built on the proton $i_{13/2}$ two-quasiparticle configuration. This orbital is a *hyper-intruder* orbital, since it originates from three shells above, and one would expect *hyper-intruder* orbitals to be occupied in hyperdeformed structures. More neutron-rich isotopes in this region seem to be an even better hunting ground for extreme deformations, however, they are extremely difficult to reach experimentally.

ACKNOWLEDGMENTS

We would like to thank the crew and staff of the ATLAS accelerator, and Andrzej Lipski (SUNY) for making the targets. This work has been supported in part by the U.S. DoE under contract Nos. DE–AC03–76SF00098 (LBNL) and W–31–109–ENG–38 (ANL). Two of us (RMC and RW) acknowledge partial support from NATO under grant CRG 972142. Discussions with Yang Sun on the projected shell model calculations are gratefully acknowledged.

REFERENCES

1. Chasman, R.R., Phys. Rev. C **64**, 024311 (2001)
2. Werner, T.R. and Dudek, J., At. Data Nucl. Data Tables **59**, 1 (1995)
3. Cromaz, M., *et al.*, Nucl. Instr. Meth. A **462**, 519 (2001)
4. Clark, R.M., *et al.*, Phys. Rev. Lett. **87**, 202502 (2001)
5. Görgen, A., *et al.*, Phys. Rev. C **65**, 027302 (2002)
6. Ward, D., *et al.*, Phys. Rev. C **66**, 024317 (2002)
7. Ziegler, J.F., Biersack, J.P., and Littmark, U., *The Stopping and Ranges of Ions in Matter*, (Pergamon, London, 1985), Vol. 1
8. Nisius, D., *et al.*, Phys. Lett. B **392**, 18 (1997)
9. Metag, V., Habs, D., and Specht, H.J., Phys. Rep. **65**, 1 (1980)
10. Hara, K. and Sun, Y., Int. J. Mod. Phys. E **4**, 637 (1995)
11. Lee, C.T., et al., Phys. Rev. C **65**, 041301(R) (2002)
12. Sun, Y., private communication